Experimental Mechanics (2014) 54:127–136
DOI 10.1007/s11340-012-9640-2

Interfacial Residual Stress Analysis of Thermal Spray Coatings by Miniature Ring-Core Cutting Combined with DIC Method

J.G. Zhu · H.M. Xie · Y.J. Li · Z.X. Hu · Q. Luo · C.Z. Gu

Received: 31 January 2012 / Accepted: 31 May 2012 / Published online: 22 June 2012

Abstract The residual stress in thermal barrier coatings (TBCs) fabricated from coating deposition plays a vital role in the coating design and processing parameters optimization. The main objective of the present work is to determine the interfacial residual stress in TBCs by means of miniature ring-core cutting and the digital image correlation (DIC) method. Both the ring-core cutting and the dot pattern used for DIC deformation measurement are implemented by the focused ion beam (FIB) milling on the cross-section of a coating. A finite element model (FEM) is developed to simulate the ring-core cutting process. From the FEM, the calibration coefficients are determined for general applications. The surface of the ring-core containing dot patterns is recorded before and after the FIB milling process. DIC technique is then performed to calculate the surface displacement caused by the release of residual stresses due to the cutting. Results demonstrate that the interfacial residual stress in TBCs is nearly in a uniaxial stress state and has a tendency to be compressive toward the interface. Finally, essential aspects of the technique are discussed.

Keywords Residual stress · Thermal barrier coatings (TBCs) · Focused ion beam (FIB) · Digital image correlation (DIC) · Ring-core cutting method

J.G. Zhu · H.M. Xie (✉) · Y.J. Li · Z.X. Hu
AML, Department of Engineering Mechanics,
Tsinghua University,
Beijing 100084, China
e-mail: xiehm@mail.tsinghua.edu.cn

J.G. Zhu
College of Civil Engineering and Mechanics, Jiangsu University,
Zhenjiang, Jiangsu 212013, China

Q. Luo · C.Z. Gu
Institute of Physics, Chinese Academic of Sciences,
Beijing 100081, China

Introduction

Thermal spray coatings are widely used to provide thermal insulation to metallic components from hot gas stream in gas-turbine engines for propulsion or power generation. It is widely recognized that residual stresses in thermal spray coatings are highly significant in practice [1, 2]. High residual stresses in TBCs could lead to cracking, delamination of the coating, shape changes, etc., and deteriorate the performance and reliability of the entire structures. As such, determination of residual stress in TBCs from thermal spray process plays a vital role in the coating design and processing parameters optimization. Considerable efforts, though difficult, have been made to estimate and understand the interfacial residual stresses introduced during the deposition of thermal spray coatings [3]. Although recently there have been important advances in understanding how these stresses arise, reliable experimental results are not easy to obtain.

Techniques of residual stress measurement in coatings can generally be divided into nondestructive and destructive ones. The nondestructive techniques usually measure parameters that are related to the stress, such as X-ray or neutron diffraction and curvature method. The X-ray or neutron diffraction probes the changes in lattice constants caused by stress [4, 5]. The main drawback of these techniques is the shallow penetration depth of the incident beam, which confines the analysis to a surface layer. In order to obtain stress/depth profile, X-ray diffraction can be combined with layer removal methods [6]. However, a progressive layer removal technique is generally unadvisable for ceramic materials where an uncontrolled stress relaxation or modification can occur. The curvature method involves measuring the bending of a strip coating or circular coating [7, 8]. The strip curvature is often readily measurable; but it is a complex task to interpret such data in terms of stress state. Although the Stoney equation has been

established to describe the stress in thin films, it is a rather difficult task to infer stress state of thermal spray coatings from curvature measurement [9–12].

The destructive techniques, such as block sectioning, slitting, hole-drilling and ring-core cutting with strain gauge rosettes, are well established due to their versatility and reliability [13–15]. The ring-core cutting method mills an annular groove to relieve residual stresses. It was reported that the ring-core cutting method can offer greater measurement sensitivity because the magnitude of relieved strains is one order of magnitude larger than that in the hole-drilling method [16]. In recent years, the full-field optical techniques such as moiré interferometry [17], electronic speckle-pattern interferometry (ESPI) [18] and digital image correlation (DIC) [19], have been used with hole-drilling to determine residual stresses from surface displacements (or strains). Among them, DIC technique offers special and attractive advantages such as simple experimental setup and specimen preparation, less stringent in measurement environment, and wide range of measurement sensitivity and resolution [20].

Note that each measurement technique has its unique characteristics in scope. On one hand, the nondestructive techniques usually have to be calibrated before measurement and the calibration coefficients are likely to be affected by the materials, inner structure of the objects etc. On the other hand, the destructive techniques will cause damage to the tested specimens [21]. The recently developed focused ion beam (FIB) cutting may be a trade-off of the above conflicts. FIB has been applied as a novel cutting/remove technique to make microscale cuts, holes, rings, slots etc. [22–24]. In addition, the scanning electron microscope (SEM) of the dual-beam system offers excellent imaging resolution for DIC analysis. These new developments dramatically extend the dimension of residual stress measurement into the micro- and nano-scale.

The purpose of the present investigation is to determine the interfacial residual stress in TBCs using the combination of FIB milling, SEM imaging, DIC analysis and FEM calibration. First, the calibration coefficients are analyzed by finite element method. Then, the experimental procedures are described including ring-core cutting using FIB milling and displacement determination by DIC method. Finally, the interfacial residual stresses are obtained followed by discussion and conclusion.

Methodology

Residual Stress Calculation: Ring-Core Cutting Method

Figure 1 illustrates the ring-core cutting method. If a ring-core cutting is through the plate thickness, the stresses around the central core are completely relieved and only the strain relaxed on the central core needs to be analyzed. For a certain point (r,θ) in polar coordinate [see Fig. 1(a)], the in-plane strains ε_r, ε_θ and $\gamma_{r\theta}$ can be derived as [16, 25]

$$\begin{bmatrix} \varepsilon_r \\ \varepsilon_\theta \\ \gamma_{r\theta} \end{bmatrix} = \frac{1}{E} \begin{bmatrix} 1-\nu & (1+\nu)\cos 2\theta & -(1+\nu)\sin 2\theta \\ 1-\nu & -(1+\nu)\cos 2\theta & (1+\nu)\sin 2\theta \\ 0 & -2(1+\nu)\sin 2\theta & -2(1+\nu)\cos 2\theta \end{bmatrix} \times \begin{bmatrix} -\frac{\sigma_1+\sigma_2}{2} \\ -\frac{\sigma_1-\sigma_2}{2}\cos\varphi \\ \frac{\sigma_1-\sigma_2}{2}\sin 2\varphi \end{bmatrix} \quad (1)$$

where E is Young's modulus and v is Poisson's ratio, σ_1 and σ_2 are the maximum and minimum principal stresses. θ and φ are defined to be positive in counterclockwise direction as shown in Fig. 1.

The radial displacement can be obtained by integrating the radial strain over the radius.

$$u(r,\theta) = \int \varepsilon_r dr = A(r)\xi + B(r)\zeta\cos[2(\varphi-\theta)] \quad (2)$$

where $\xi = -(\sigma_1+\sigma_2)/2$, $\zeta = -(\sigma_1-\sigma_2)/2$, $A(r) = (1-\nu)r/E$ and $B(r) = (1+\nu)r/E$. $A(r)$ and $B(r)$ are coefficients in terms of the radius r, Young's modulus E and Poisson's ratio v. These parameters are taken into account by finite element method in the "Determination of Calibration Coefficients by FEA". Equation (2) indicates that the three unknowns (σ_1,$\sigma_2$and φ) can be determined using three measured displacements. In order to make full use of the test data,

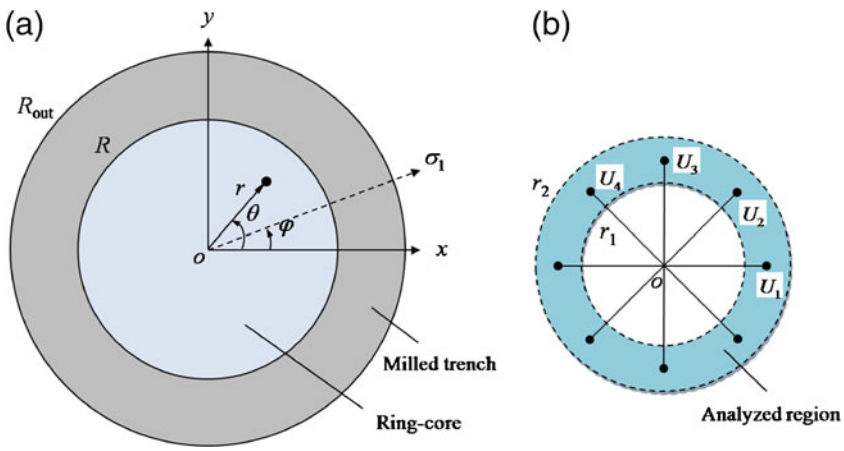

Fig. 1 Schematic diagram of the ring-core cutting method. (**a**) Coordinate configurations. σ_1 is the maximum principal stress. Both θ and φ are defined to be positive in counterclockwise direction. R and R_{out} are the inner and outer radii of the annular ring, respectively. (**b**) Measurement configurations. The analyzed region is bounded by inner and outer radii r_1 and r_2 ($r_1<r_2<R$)

four values of the relieved displacements (U_1, U_2, U_3 and U_4) are used and each is measured between two points, which are determined at the intersection of a circle of radius r and a line crossing the center of the core[see Fig. 1(b)]. Therefore, the relieved displacements can be expressed compactly in matrix form as follows

$$\begin{bmatrix} U_1(r) \\ U_2(r) \\ U_3(r) \\ U_4(r) \end{bmatrix} = \begin{bmatrix} A(r) & B(r) & 0 \\ A(r) & 0 & B(r) \\ A(r) & -B(r) & 0 \\ A(r) & 0 & -B(r) \end{bmatrix} \begin{bmatrix} L \\ M \\ N \end{bmatrix} \tag{3}$$

$$L = -(\sigma_1 + \sigma_2), M = -(\sigma_1 - \sigma_2)\cos(2\varphi) \text{ and} \tag{4}$$
$$N = -(\sigma_1 - \sigma_2)\sin(2\varphi)$$

where $U_1(r) = 2u(r, \theta = 0^o)$, $U_2(r) = 2u(r, \theta = 45^o)$, $U_3(r) = 2u(r, \theta = 90^o)$ and $U_4(r) = 2u(r, \theta = 135^o)$. Note in equation (3) four displacements are written to determine three unknowns L,M and N, as displacements from four points were used in the experiment. Although three is minimum, the number of displacements can be more than three to determine the three unknowns in least-square sense.

Determination of Calibration Coefficients by FEA

The coefficients, A and B, can be determined by three-dimensional finite element analysis, in which the material constants and the geometrical parameters of the ring-core have to be taken into account. To simulate the removal of the ring material, normal and shear tractions are applied to the inner and outer walls of the ring core. At any arbitrary angle, the tractions applied to the inner and outer walls have the same magnitudes but opposite directions. The calibration coefficients A and B can be determined by using two loading conditions:

(1) $\sigma_1 = \sigma_2 = \sigma$, an equibiaxial residual stress field, which is equivalent to a uniform pressure $p=\sigma$, acting on the inner and outer walls of the ring core as shown in Fig. 2(a). By using equation (2), the coefficient A can be determined as

$$A\left(E, v, \frac{r}{R}, \frac{h}{R}\right) = -\frac{u_r(r,\theta)}{\sigma} \tag{5}$$

where h is the trench depth.

(2) $\sigma_1 = -\sigma_2 = \sigma$, a pure shear residual stress field, which is equivalent to a harmonic distribution of the normal stress $\sigma_{rr} = -\sigma\cos 2\theta$and the shear stress $\tau_{r\theta} = \sigma \sin 2\theta$, acting on the inner and outer walls of the ring core as shown in Fig. 2(b). By using equation (2), the coefficient B can be determined as

$$B\left(E, v, \frac{r}{R}, \frac{h}{R}\right) = -\frac{u_r(r,\theta)}{\sigma\cos 2(\theta - \varphi)} \tag{6}$$

In equations (5, 6), $u_r(r,\theta)$ is the surface displacement calculated from the finite element analysis. It can be seen that the calibration coefficients A and B are dependent on the material constants (Young's modulus E and Poisson ratio v) and the geometrical parameters (the inner radius R, the outer radius R_{out}, trench depth-to-inner radius ratio h/R and the radial coordinate-to-inner radius ratio r/R). For model with $R_{out}>2R$, the coefficients show little dependence on the variation of outer radius. Therefore, the variation of R_{out} is not considered in the calibration. The coefficients can be converted into nondimensional parameters so that they can be used for different materials.

$$A' = \frac{E}{(1-v)R}A, \; B' = \frac{E}{(1+v)R}B \tag{7}$$

A three-dimensional finite element model of 8-node isotropic brick element C3D8 was established by using the commercial code ABAQUS 6.9. The parameters used in the analysis were σ=1 MPa; E=100 GPa; v=0.25, R= 2 μm and R_{out}=4 μm. The elements of the ring-core were removed to simulate the FIB milling. And then, the specified loading condition was applied at the inner and outer wall of the trench. After calculation, the displacement response on the pillar surface can be obtained as shown in Fig. 3. According to equations (5–7), the calibration coefficients as functions of normalized radial coordinate and normalized trench depth are shown in Figs. 4 and 5.

As can be seen from Fig. 4, the coefficient increases with increasing r/R. This implies that it is essential to use the data at the points very close to the pillar boundary to achieve high accuracy of residual stress measurement. However, it is reasonable to use proper value of normalized r/R to avoid the uncertainties associated with re-depositions or surface

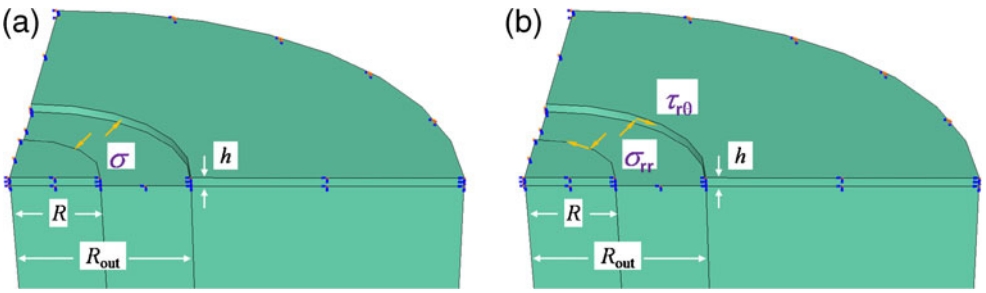

Fig. 2 Finite element models of loading conditions: (**a**) a uniform pressure and (**b**) a pure shear stress. Only one quarter of the specimen is modeled due to the symmetric reason

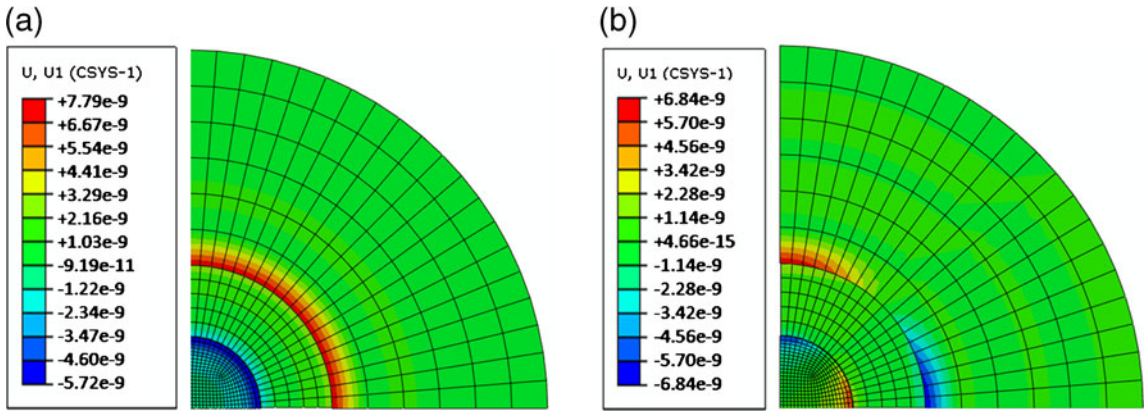

Fig. 3 Distributions of radial displacement fields under the loading condition of (**a**) a uniform pressure and (**b**) a pure shear stress

damages on the upper surface of pillar boundary caused by FIB milling. In addition, as can be seen from Fig. 5, the coefficients increase initially as normalized h/R increases and remain stable when the trench depth-to-inner radius ratio reaches 1.2, which implies that full relief is reached and further milling depth is not necessary.

Experimental Procedures

Coating Deposition

The thermal spray coatings consisted of a top coating and a bond coating attached to a 304 stainless steel substrate (thickness of 2 mm). The chemical composition of the bond coating was Ni58Cr17Al2.8Y powder (weight percentage) with thickness of 100 μm. The top coating was a 500 μm thick ZrO_2-8wt%Y_2O_3 (YSZ). The spraying process was carried out using an APS-2000 equipment at the Institute of Process Engineering, Chinese Academy of Science in Beijing. The steel substrate was firstly exposed to a grit-blasting treatment to roughen the surface prior to deposition to allow better coating adhesion. Then, the coatings were deposited on the substrate in an ambient atmosphere with an automated single-gun plasma-spray process. The parameters of atmospheric plasma spraying and grit blasting are listed in Table 1. After that, the cross-section of the thermal spray coatings was finely polished and observed under the scanning electron microscope. And the SEM image of TBCs' cross-section is shown in Fig. 6.

FIB Relaxation Procedures

All the experiments were conducted under the FEI DB 235 system with the FIB-SEM dual beams. A schematic diagram of experimental procedures is shown in Fig. 7. It should be noted that two modes (mode 1 and mode 2) were used in the experiments. When in mode 1, the FIB gun is normal to the sample for FIB sputtering or milling, and the SEM gun tilts an angle of 45°. When in mode 2, the SEM gun is normal to the sample and the FIB gun tilts.

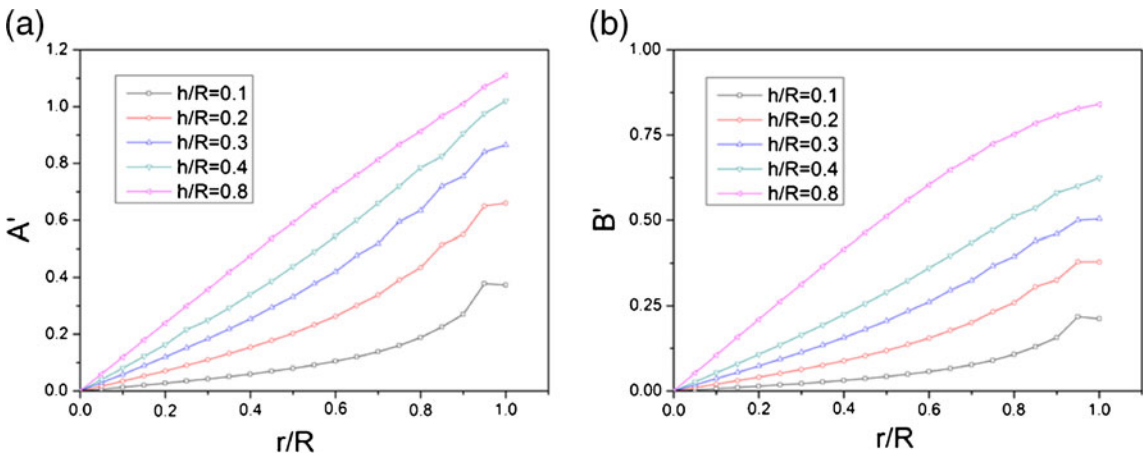

Fig. 4 Calibration coefficients (**a**) A' and (**b**) B' as a function of normalized radial coordinate r/R

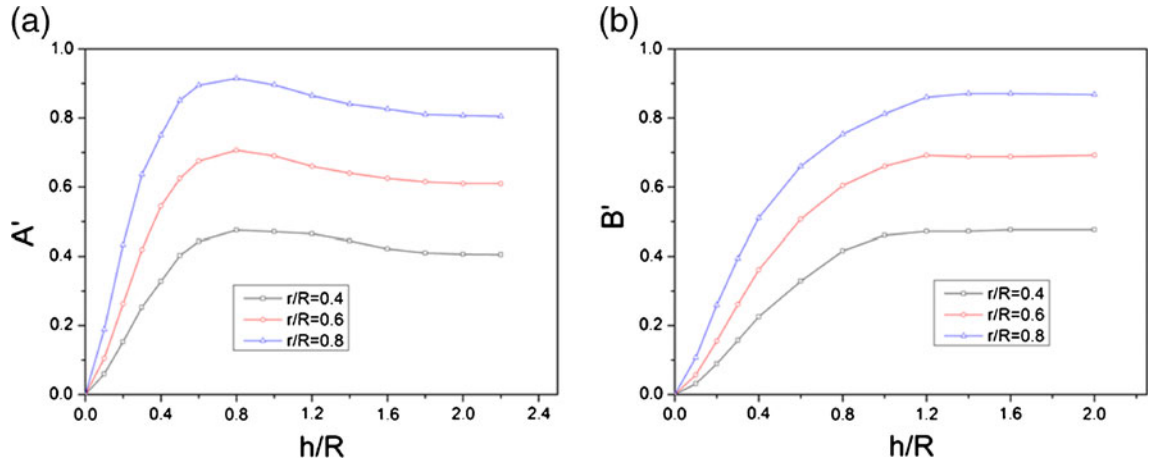

Fig. 5 Calibration coefficients (**a**) A' and (**b**) B' as a function of normalized trench depth h/R

First, mode 1 was used and a 100 nm platinum layer was deposited by FIB deposition on the cross section of the non-conductive ceramic coatings. The Pt layer not only can increase the electrical conductivity of the sample for FIB milling and SEM imaging, but also create a homogeneous surface for the milling of the patterned dots. Then, a further thin circular ring of platinum (diameter of about 4 μm) was deposited to preserve the shape of the edge during FIB milling and to protect the central surface from re-deposition during FIB operations.

Subsequently, a matrix of small dots (diameter and depth of about 100 nm, interval of about 350 nm) was milled within the circular ring at a current of 50 pA at 30 kV. These patterned dots would be used as the deformation carriers of sample surface. An example of patterned dots imaged with tilted SEM is shown in Fig. 8(a).

At this point, mode 1 was changed to mode 2 and a high resolution micrograph of the milled pattern was acquired before ion-beam milling at the magnification of 35,000× to serve as a reference for displacement calculation. A typical example of the reference micrograph before milling is shown in Fig. 9(a).

After the reference micrograph was acquired, mode 2 was changed back to mode 1 and ring-core FIB milling was then performed at a current of 1000 pA at 30 kV. The depth was set as 2 μm, while the inner and outer diameter of the trench was set as 4 μm and 8 μm, respectively. After FIB milling, the sample surface was observed, and Fig. 8(b) presents a patterned surface after milling with tilt angle of 45°. The actual milling depth and pillar diameter were accurately measured by image analysis on the SEM micrographs.

Finally, mode 1 was changed to mode 2 again and a high resolution SEM micrograph was acquired with the same parameters as the original reference image, which is to serve as a deformed image for displacement calculation. A typical example of the deformed micrograph after milling is shown in Fig. 9(b).

The overall duration of one single test (mainly the trench milling) was less than 40 min for a pillar diameter of 4 μm (some variation is expected depending on the specified coating material).

Displacement Measurement by 2D DIC

2D digital image correlation is an in-plane displacement measurement technique which correlates a pair of digital speckle patterns obtained at two different loading conditions and searches for the maximum correlation coefficient C [26].

Table 1 Parameters of atmospheric plasma spray and grit blasting

Atmospheric plasma spray	Coating layer	Top coating	Bond coating
	Chemical composition	ZrO_2-8wt%Y_2O_3	NiCrCoAlY
	Arc voltage	70 V	60 V
	Arc current	500 A	400A
	Spraying distance	125 mm	125 mm
	Torch moving velocity	300 mm/s	300 mm/s
	Powder feed rate	30 g/min	30 g/min
Grit blasting	Material	Corundum	
	Particle size	2 mm	
	Pressure	0.7 MPa	
	Distance	120 mm	

$$C=\sum_{i=1}^{m}\sum_{j=1}^{n}\left[\frac{f(x_i,y_i)-f_m}{\sqrt{\sum_{i=1}^{m}\sum_{j=1}^{n}[f(x_i,y_i)-f_m]^2}}-\frac{g(x_i',y_i')-g_m}{\sqrt{\sum_{i=1}^{m}\sum_{j=1}^{n}[g(x_i',y_i')-g_m]^2}}\right]^2 \tag{8}$$

where $f(x_i,y_i)$ and $g(x_i',y_i')$ are the gray-levels at points (x_i,y_i) and (x_i',y_i') on the sub-images before and after loading, respectively. f_m and g_m are the mean intensity values of reference and target subsets, respectively. The above Zero-Normalized Sum of Squared Differences (ZNSSD) correlation criterion is insensitive to the scale and offset of illumination lighting fluctuations [27]. And the correlation function can be optimized using the iterative Newton–Rapshon (NR) method to resolve the deformation parameters. To achieve sub-pixel accuracy, the correlation algorithms use gray value interpolation. Generally, more accurate displacement information can be obtained with higher-order interpolation methods. The currently implemented interpolation method is the bi-cubic spline interpolation.

In order to determine the residual stress in combination with the ring-core cutting method in equation (3), the values of the relieved displacements (U_1, U_2, U_3 and U_4) were measured by 2D DIC technique in the analyzed region bounded by inner and outer radii r_1 and r_2 ($r_1<r_2<R$).

Results

In order to evaluate the interfacial residual stress of the topcoat, three areas of about 10 μm^2 on the cross-section of the topcoat near the TBC/BC interface were selected for ring-core FIB milling in consideration of avoiding micro-pores and cracks. Specific parameters are listed in Table 2.

In the experiment, the inner radius was 2 μm to reduce the effects of the microdefects (such as micro cracks and pores) on the relaxation mechanisms. This radius assures that the basic assumptions of continuum mechanics remain valid at the scales used in the study. The average milling depth of the trench is about 2.4 μm, which satisfies $h/R=1.2$ and the displacement is relaxed almost completely based on the relaxation curves in Fig. 5.

According to the micrographs of the patterned surface before and after milling, the radial displacements of milled dots were calculated using the 2D DIC technique. In equation (3), the displacements of points at the same radius coordinate ($0.5<r/R<0.8$) were measured from DIC techinique and

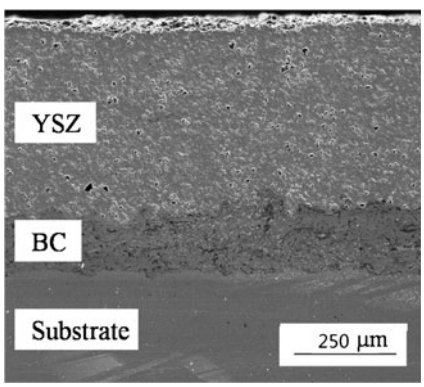

Fig. 6 SEM image of the TBC cross-section

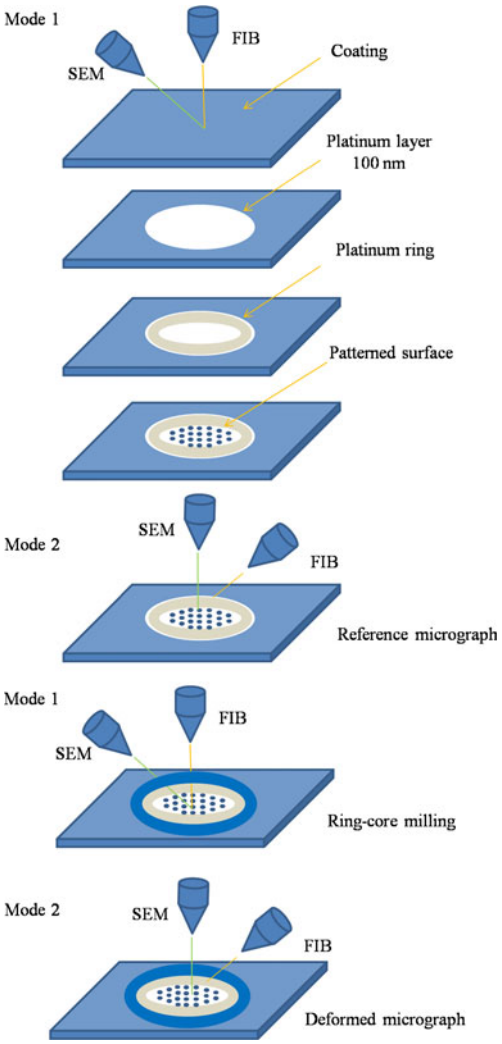

Fig. 7 Schematic diagram of experimental procedures for residual stress measurement by FIB milling

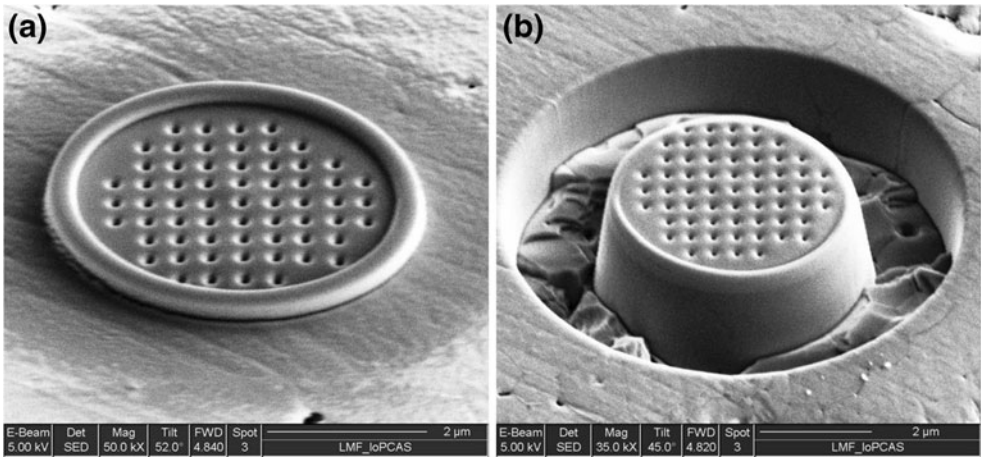

Fig. 8 SEM diagrams of the patterned surface (**a**) before milling and (**b**) after milling

listed in Table 2. In addition, the magnitudes of coefficients A and B at the same radius coordinate ($0.5<r/R<0.8$) in Fig. 5 were also used in residual stress calculation.

By solving equation (3), the three unknowns (σ_1, σ_2 and φ) were obtained. The calculated results are listed in Table 2. Each magnitude of σ_1 is almost ten times that of σ_2, which indicates that the interfacial residual stress in the cross-section of thermal spray coatings is nearly in a uniaxial stress state. The first principle stresses (σ_1) are positive, which manifests that residual stress is compressive because the sign of residual stress is opposite to the measured stress released by the ring-core cutting method. In addition, the small absolute value of φ implies that σ_1 is mainly parallel with the interface. The maximum compressive stress is 450 MPa, which is similar to the results measured by the nanoindentation [28, 29]. Furthermore, the residual stress in TBC is not uniformly distributed across the thickness, which has a tendency to be a compressive stress state toward the interface. The results agree with that reported in [30, 31]. Residual stress in plasma sprayed coating originates from the rapid solidification and eventual cooling of molten droplets spread on a substrate. As studied by Clyne [9], the compressive stress is introduced mainly due to the mismatch of the thermal strains from the substrate and the ceramic coatings after the coating depositions. And a tendency to a more compressive stress state toward the substrate is associated with the progressively coating deposition and layer-by-layer buildup of coatings.

Discussion

As illustrated in Fig. 8, a platinum ring was purposely deposited before milling mainly to preserve the shape of the pillar edge and to protect the central surface from re-deposition during FIB operations. Figure 10 shows the SEM diagram of patterned surface on the ring core without Pt-ring deposition before milling. It can be seen that the pillar edge is collapsed and most of all, the patterned surface is ambiguous. Compared with Fig. 8, the deposition of Pt-ring proves to be successful before milling to enhance the image definition and quality.

When the ring-core method is used on the coating surface, the in-plane equi-biaxial stress state is assumed. And the coefficients calibration can be simplified by using an axisymmetric model [23]. As for arbitrary stress state, however, the coefficients should be calibrated with different

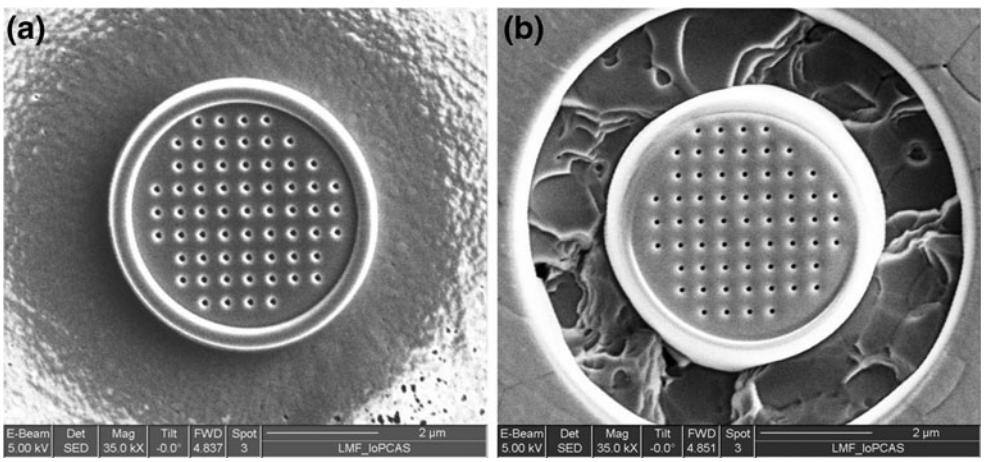

Fig. 9 Typical example of ring-core FIB milling procedure: (**a**) reference micrograph of the patterned surface before milling and (**b**) deformed micrograph of the patterned surface after milling

Table 2 Parameters and calculated results of ring-core FIB milling

No.	l (μm)	R (μm)	Rout (μm)	h (μm)	$U1$ (nm)	$U2$	$U3$	$U4$	σ_1 (MPa)	σ_2 (MPa)	φ (deg)
1#	20	2	4	2.4	-7.2	3.9	-0.5	-11.7	441.4	-43.1	5.7
2#	100			2.5	3.7	-2.0	-10.4	-4.7	378.1	-34.6	-10.9
3#	200			2.3	0.7	-4.6	-6.6	-1.3	267.2	36.9	4.5

l: Distance to the TBC/BC interface; R and R_{out} are the inner and outer radius respectively

U1, U2, U3 and *U4* are determined at r/R=0.8

loading conditions by the transformation from rectangular coordinates to cylindrical coordinates. In addition, the coefficients were calibrated using the surface displacement rather than surface strain. Although strain field can be obtained by differentiating of the displacement map in theory, the numerical differentiation is considered as an unstable and risky operation [20] . Furthermore, the accuracy of the calculated strain is likely to be affected by the size of strain calculation window. The displacement calibration is therefore considered to be more reliable than the strain calibration.

Similar to the incremental hole-drilling method [17, 32], the ring-core cutting method can also be combined with the incremental relaxation technique to explore the stress/depth profile as reported in [16, 33]. Since ceramic coatings are hard matters, it is very different to conduct the incremental hole-drilling mechanically. At the same time, it is not possible to perform the incremental milling on the top surface of thermal barrier coatings with a typical thickness of 200–500 μm [34]. Besides, mode 1 must be kept throughout the incremental milling process and the SEM images of the patterned surface are always tilted, which may bring errors and add additional calculations to obtain the radial displacement. Since this article aims to explore the interfacial residual stress of thermal spray coatings, only one milling relaxation was performed for full stress relief. The performance not only can reduce the experimental errors but also avoid mathematical ill-conditioning related to the inverse solutions [21, 35]. It should be noted that the stress measurement technique at the microscopic scale has a potential to evaluate the interfacial residual stress at the key positions of thermal barrier coatings. For example the areas of stress concentration of the interfacial undulations and the induced stress developed due to thermal cycling [1].

The stress/depth profile of multilayer film/structure is an interesting topic for research, especially the interfacial stresses which may pose a major threat to the integrity and performance of the entire structures. Both the numerical predictions [12, 36, 37] and the experimental measurements [29, 38] have demonstrated that the stress state in the top thermally sprayed coatings has a tendency to be compressive toward the interface. The numerical analyses based on the elastic–plastic model predict an almost linear stress gradient through the thickness of the top coating [12, 36, 37]. However, the nonlinear gradient of stress level in the top ceramic coatings evaluated by the experimental measurements seems more complicated than the numerical predictions [29, 38]. This is perhaps associated with the inhomogeneous mechanical properties, such as elastic modulus, thermal expansion, yielding strength etc., influenced by temperature gradient during the coating deposition. It should be noted that the porous ceramic coating includes micro-voids and cracks, the experimental results therefore are the combination of ceramic material and surrounding micro-pores.

It can be seen from equation (3) that the accuracy of measured values of σ_1, σ_2 and φ relies heavily on the accuracy of calibration coefficients determined by FEA and the accuracy of displacement computed by the DIC technique. Since the former factor can easily be controlled by the use of a dense mesh in FEA, the accuracy of measured values of σ_1, σ_2 and φ mainly depends on displacement estimation accuracy. Normally, the accuracy of the displacement estimation using the NR algorithm can achieve±0.02 pixels. In this experiment, 1 pixel equals to 8 nm, as shown in Figs. 8 and 9 thus, the corresponding displacement error is about±0.16 nm. Nevertheless, the theoretical analysis of displacement error is affected by multiple factors, for example image distortions, speckle pattern and noise [20].

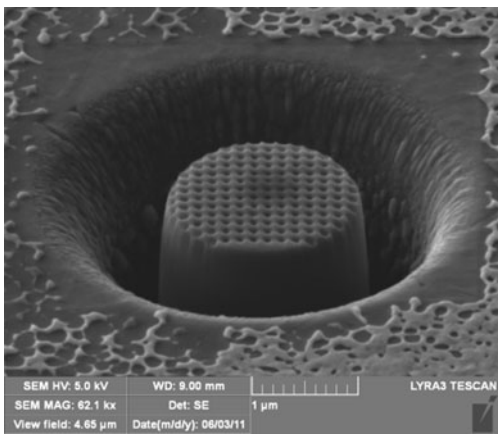

Fig. 10 SEM diagram of patterned surface on the ring core without Pt-ring deposition before milling

Conclusion

The present study provides a detailed description of interfacial residual stress analysis of thermal spray coatings by a combined miniature ring-core cutting and DIC method. Specific findings can be summarized as follows:

(1) A new methodology for interfacial residual stress measurement at the microscopic scale by the combination of FIB milling, SEM imaging, DIC analysis and FEM calibration was proposed and it has a potential to evaluate the interfacial residual stress at the key positions thermal barrier coatings.
(2) The stress state on the cross-section of thermal spray coatings in the vicinity of the TBC/BC interface was determined by the above method. The results demonstrate that the interfacial residual stress is nearly in a uniaxial stress state (compressive) parallel with the interface and has a tendency to be more compressive toward the interface.
(3) The experimental procedure was carefully designed to ensure the reliability of the method. It may be automated for residual stress determination at the microscopic scale.
(4) Finite element simulations were carried out to investigate the displacement relief caused by ring drilling for arbitrary stress state. It is generally believed that the displacement calibration is more reliable than the strain calibration.
(5) The accuracy of experimental measurement was discussed and it relies mainly on the accuracy of displacement measured by the DIC technique. The theoretical displacement error is only about±0.16 nm.

Acknowledgements The authors are grateful to the financial supported by the National Basic Research Program of China ("973" Project) (Grant No.2010CB631005, 2011CB606105), the National Natural Science Foundation of China (Grant Nos. 11172151, 90916010), Specialized Research Fund for the Doctoral Program of Higher Education (Grant No.20090002110048).

References

1. Evans AG, Mumm DR, Hutchinson JW, Meier GH, Pettit FS (2001) Mechanisms controlling the durability of thermal barrier coatings. Prog Mater Sci 46(5):505–553
2. Johnston RE (2009) The sensitivity of abradable coating residual stresses to varying material properties. J Therm Spray Technol 18 (5–6):1004–1013. doi:10.1007/s11666-009-9378-2
3. Rabiei A, Evans AG (2000) Failure mechanisms associated with the thermally grown oxide in plasma-sprayed thermal barrier coatings. Acta Mater 48(15):3963–3976
4. Matejicek J, Sampath S, Dubsky J (1998) X-ray residual stress measurement in metallic and ceramic plasma sprayed coatings. J Therm Spray Technol 7(4):489–496
5. Matejicek J, Sampath S (2001) Intrinsic residual stresses in single splats produced by thermal spray processes. Acta Mater 49 (11):1993–1999
6. Greving DJ, Rybicki EF, Shadley JR (1994) Through-thickness residual-stress evaluations for several industrial thermal spray coatings using a modified layer-removal method. J Therm Spray Technol 3(4):379–388
7. Wenzelburger M, López D, Gadow R (2006) Methods and application of residual stress analysis on thermally sprayed coatings and layer composites. Surf CoatTechnol 201(5):1995–2001
8. Liao H, Vaslin P, Yang Y, Coddet C (1997) Determination of residual stress distribution from in situ curvature measurements for thermally sprayed WC/Co coatings. J Therm Spray Technol 6 (2):235–241
9. Clyne T, Gill S (1996) Residual stresses in thermal spray coatings and their effect on interfacial adhesion: a review of recent work. J Therm Spray Technol 5(4):401–418. doi:10.1007/bf02645271
10. Kesler O, Finot M, Suresh S, Sampath S (1997) Determination of processing-induced stresses and properties of layered and graded coatings: experimental method and results for plasma-sprayed Ni-Al_2O_3. Acta Mater 45(8):3123–3134
11. Matejicek J, Sampath S (2003) In situ measurement of residual stresses and elastic moduli in thermal sprayed coatings—Part 1: apparatus and analysis. Acta Mater 51(3):863–872. doi:10.1016/s1359-6454(02)00478-0
12. Zhu JG, Xie HM, Hu ZX, Chen PW, Zhang QM (2011) Residual stress in thermal spray coatings measured by curvature based on 3D digital image correlation technique. Surf CoatTechnol 206 (6):1396–1402
13. Khan AN, Lu J, Liao H (2003) Effect of residual stresses on air plasma sprayed thermal barrier coatings. Surf CoatTechnol 168(2–3):291–299
14. Valente T, Bartuli C, Sebastiani M, Loreto A (2005) Implementation and development of the incremental hole drilling method for the measurement of residual stress in thermal spray coatings. J Therm Spray Technol 14(4):462–470. doi:10.1361/105996305X76432
15. Santana YY, La Barbera-Sosa JG, Staia MH, Lesage J, Puchi-Cabrera ES, Chicot D, Bemporad E (2006) Measurement of residual stress in thermal spray coatings by the incremental hole drilling method. Surf CoatTechnol 201(5):2092–2098. doi:10.1016/j.surfcoat.2006.04.056
16. Li KY, Ren W (2007) Application of miniature ring-core and interferometric strain/slope rosette to determine residual stress distribution with depth - part I: theories. J Appl Mech-Trans ASME 74(2):298–306. doi:10.1115/1.2198251
17. Wu Z, Lu JA, Han BT (1998) Study of residual stress distribution by a combined method of moire interferometry and incremental hole drilling, part I: theory. J Appl Mech-Trans ASME 65(4):837–843
18. Steinzig M, Ponslet E (2003) Residual stress measurement using the hole drilling method and laser speckle interferometry: Part I. Exp Techniques 27(3):43–46
19. Lord JD, Penn D, Whitehead P (2008) The application of digital image correlation for measuring residual stress by incremental hole drilling. Appl Mech Mater 13–14:65–73
20. Pan B, Qian KM, Xie HM, Asundi A (2009) Two-dimensional digital image correlation for in-plane displacement and strain measurement: a review. Meas Sci Tech 20(6):doi:10.1088/0957-0233/20/6/062001
21. Schajer G (2010) Relaxation methods for measuring residual stresses: techniques and opportunities. Exp Mech 50(8):1117–1127. doi:10.1007/s11340-010-9386-7
22. McCarthy J, Pei Z, Becker M, Atteridge D (2000) FIB micromachined submicron thickness cantilevers for the study of thin film properties. Thin Solid Films 358(1–2):146–151

23. Korsunsky AM, Sebastiani M, Bemporad E (2009) Focused ion beam ring drilling for residual stress evaluation. Mater Lett 63 (22):1961–1963
24. Winiarski B, Langford RM, Tian JW, Yokoyama Y, Liaw PK, Withers PJ (2010) Mapping residual stress distributions at the micron scale in amorphous materials. Metall Mater Trans A 41 (7):1743–1751. doi:10.1007/s11661-009-0127-4
25. McGinnis MJ, Pessiki S, Turker H (2005) Application of three-dimensional digital image correlation to the core-drilling method. Exp Mech 45(4):359–367. doi:10.1177/0014485105055435
26. Pan B, Xie HM, Hua T, Asundi A (2009) Measurement of coefficient of thermal expansion of films using digital image correlation method. Polymer Test 28(1):75–83. doi:10.1016/j.polymertesting.2008.11.004
27. Pan B, Xie HM, Guo ZQ, Hua T (2007) Full-field strain measurement using a two-dimensional Savitzky-Golay digital differentiator in digital image correlation. Opt Eng 46(3):doi:10.1117/1.2714926
28. Zhao X, Xiao P (2006) Residual stresses in thermal barrier coatings measured by photoluminescence piezospectroscopy and indentation technique. Surf CoatTechnol 201(3–4):1124–1131. doi:10.1016/j.surfcoat.2006.01.035
29. Zhu JG, Xie HM, Hu ZX, Chen PW, Zhang QM (2012) Cross-sectional residual stresses in thermal spray coatings measured by moire' interferometry and nanoindentation technique. J Therm Spray Technol. doi:10.1007/s11666-012-9732-7
30. Montay G, Cherouat A, Lu J, Baradel N, Bianchi L (2002) Development of the high-precision incremental-step hole-drilling method for the study of residual stress in multi-layer materials: influence of temperature and substrate on ZrO_2-Y_2O_3 8 wt.% coatings. Surf Coat-Technol 155(2-3):152–160
31. Scardi P, Leoni M, Bertini L, Bertamini L, Cernuschi F (1998) Strain gradients in plasma-sprayed zirconia thermal barrier coatings. Surf CoatTechnol 108–109:93–98
32. Wu Z, Lu JA, Han BT (1998) Study of residual stress distribution by a combined method of moire interferometry and incremental hole-drilling, part II: implementation. J Appl Mech-Trans ASME 65(4):844–850
33. Ren W, Li KY (2007) Application of miniature ring-core and interferometric strain/slope rosette to determine residual stress distribution with depth—part II: experiments. J Appl Mech-Trans ASME 74(2):307–314. doi:10.1115/1.2198252
34. Padture NP, Gell M, Jordan EH (2002) Thermal barrier coatings for gas-turbine engine applications. Science 296(5566):280–284
35. Schajer GS (2010) Advances in hole-drilling residual stress measurements. Exp Mech 50(2):159–168
36. Tsui YC, Clyne TW (1997) An analytical model for predicting residual stresses in progressively deposited coatings Part 1: planar geometry. Thin Solid Films 306(1):23–33
37. Hu YY, Huang WM (2004) Elastic and elastic-plastic analysis of multilayer thin films: closed-form solutions. J Appl Phys 96 (8):4154–4160. doi:10.1063/1.1786339
38. Zhao X, Xiao P (2006) Residual stresses in thermal barrier coatings measured by photoluminescence piezospectroscopy and indentation technique. Surf CoatTechnol 201(3–4):1124–1131